IEEE Access
Multidisciplinary | Rapid Review | Open Access Journal

Received 6 October 2022, accepted 17 October 2022, date of publication 21 October 2022, date of current version 27 October 2022.

Digital Object Identifier 10.1109/ACCESS.2022.3216300

RESEARCH ARTICLE

Heat Transfer Challenges for MVDC Power Cables Used in Wide Body All Electric Aircraft Under Low Pressures

ARIAN AZIZI[1], (Member, IEEE), MONA GHASSEMI[1], (Senior Member, IEEE), AND JANE M. LEHR[2], (Fellow, IEEE)

[1]Department of Electrical and Computer Engineering, The University of Texas at Dallas, Richardson, TX 75080, USA
[2]Department of Electrical and Computer Engineering, University of New Mexico, Albuquerque, UM 87131, USA

Corresponding author: Mona Ghassemi (mona.ghassemi@utdallas.edu)

This work was supported in part by the Advanced Research Projects Agency-Energy (ARPA-E), U.S. Department of Energy, under Award DE-AR0001465.

ABSTRACT Power cables are a vital component of the future electric power systems (EPS) envisaged in wide body all electric aircraft (AEA). They are required to be high power delivery and low system mass. Designing proper power cables for AEA faces thermal challenges due to the lower pressure of 18.8 kPa at the cruising height of a wide body aircraft. Due to the limited heat transfer at that pressure, the temperature field distribution across the aircraft cable, mainly a function of pressure, surface emissivity, and ambient surface geometry, is likely to diverge from that at atmospheric pressure. Moreover, temperature field distribution affects the conductivity of the insulation, which in turn alters and may inverse the electric field distribution across the DC cables. Therefore, a coupled multi-physics study should be conducted to calculate the temperature field and electric field across the cable at different ambient temperatures and various possible geometries of the ambient environment. In this paper, the temperature field distribution across a 5 kV DC cable is studied at atmospheric and 18.8 kPa pressures. The voltage level of 5 kV was resulted from our previous studies where we proposed new EPS architectures for a wide-body AEA. The main purpose of this study is to obtain the maximum permissible current flowing the cable at the atmospheric and 18.8 kPa pressures regarding the thermal limits of the cable. It is shown that at 18.8 kPa the maximum permissible current flowing the cable is decreased by 14.75% compared to its value at atmospheric pressure when the size of the ambient surface is 250 mm. Also, the electric conductivity and electric field across the cable insulation are evaluated at different conductor currents and insulator temperature gradients.

INDEX TERMS Aircraft electrification, all electric aircraft (AEA), MVDC power cable, electric power system (EPS), finite element model (FEM), heat convection, thermal analysis.

I. INTRODUCTION

Electrification of commercial aircraft has been the subject of substantial research in recent decades to replace mechanical, hydraulic, and pneumatic systems with electrical systems to achieve more electric aircraft (MEA). In all electric aircraft (AEA), the propulsion system is also replaced with an electric system utilizing electrochemical energy instead of fuel.

The associate editor coordinating the review of this manuscript and approving it for publication was Fanbiao Li.

To achieve electrification of commercial aircraft, an electric power system (EPS) with high power delivery and low system mass is required to make the power density of MEA and AEA closer to that of conventional aircraft [1], [2], [3], [4]. An aircraft EPS is an isolated microgrid containing power electronic components, electric machines, electrochemical energy units, different loads, etc., that are connected via power cables.

Operating at a higher voltage is an approach to reduce the weight of cables, hence the overall mass of the aircraft EPS.

In our previous studies [4], [5], [6], [7], new EPS architectures for an envisaged wide body AEA were introduced and studied where the main part of aircraft EPS is an MVDC network at ±5 kV voltage level. However, the design of ±5 kV power cables for the architectures that can operate at low pressures has not been done yet. The power cables operating at ±5 kV voltage and lower pressure meet challenges such as arcing, partial discharge (PD), surface charges, thermal management, and conductor material [2].

Arcs that form in EPSs used in aircraft might be disastrous; thus, they should be avoided or managed at the very least [8]. Using aluminum conductors and a DC supply voltage increase the risk and possible damage of occurring arcing [9], [10]. Consequently, it is necessary to choose the cables' insulating material appropriately. The temperature field of DC cables influences PD behavior, such as repetition rate and occurrence in cavities during transients and PD inception voltage [11], [12]. Moreover, before choosing a cable system, PD tests must be performed to determine whether high operating temperatures caused by high currents might accelerate the aging of the cables [13]. Electrostatic discharges could occur because of surface charges on certain insulating materials. Hydrogen, which might be used as an AEA's energy source, could be ignited by discharges with relatively little energy [2]. Thermal management is of great importance as the cable dimensions, weight, and the maximum current flowing through the cable conductor are highly dependent on the thermal characteristics of the cable [14]. The thermal behavior of the power cables used in aircraft EPSs is significantly influenced by strongly limited heat convection at lowered air pressure i.e., air pressure of 18.8 kPa at cruising altitude (12.2 km) of a wide body aircraft [15]. Therefore, the maximum permissible current flowing the cable conductor is different from that of atmospheric pressure. To optimize the design of a ±5 kV voltage cable for aircraft EPS, it is desired to study the temperature field of the cable at lower pressures to obtain the maximum current flowing through the cable conductor.

The distribution of temperature fields across the cable insulation is also critical for obtaining electric field distribution. The conductivity of DC cables, which is a strong function of temperature and electric field, determines the electric field. Also, space charge accumulation is caused by the conductivity gradient across the insulation which in turn depends on the temperature gradient. Space charge accumulation affects the electric field distribution and potentially causes dielectric degradation and failure [16], [17], [18]. Accumulation of the space charge in polymeric insulation materials will accelerate beyond their electric field threshold [19]. It is critical to keep the electric field in the cable below the threshold to ensure a safe and reliable extended service life for the cables in DC operation. However, the electric field threshold for cross-linked polyethylene (XLPE) and ethylene propylene diene monomer (EPDM) rubber reduces when the temperature of the insulation increases [17], [20], [21]. Therefore, obtaining the temperature field precisely throughout the cable provides insight into building a DC cable with a very high level of safety and dependable long-life operation required in aircraft. However, to the best of our knowledge, no paper has been studying the temperature field and electric field of an aircraft MVDC power cable at a reduced pressure of air. All done to date have been for underground or submarine cables. For example, in [22], COMSOL software was used to conduct a coupled multi-physics analysis to determine the temperature and electric field distribution across an underground XLPE cable. Authors in [23] conducted a numerical analysis on a DC cable to determine partial discharge (PD) characteristics considering the effects of the temperature gradient, and although the cable is exposed to air, the natural heat convection was modeled by a convective heat flux. In [24] electrical degradation of an XLPE cable was obtained by using COMSOL software. The paper, however, neglected the ambient environment of the cable. Authors in [25] optimize the ampacity of a submarine HVDC cable taking into consideration of water flow.

TABLE 1. 5 kV no lead ethylene propylene rubber (NL-EPR) cable geometrical characteristics [26].

Parameters	Value
Conductor Overall Diameter (mm)	28.372
Insulation Overall diameter (mm)	34.341
PVC Jacket Thickness (mm)	2.032
Cable Overall Diameter (mm)	40.439
Rated temperature for normal operation (°C)	105

In this paper, a finite element method (FEM) model of a 5 kV in the COMSOL software is developed to determine the temperature field and electric field distributions across the cable. The major aim is to calculate the maximum permissible current flowing the cable at the atmospheric and reduced pressure of 18.8 kPa concerning the thermal and electrical limits of the cable. Analyzing the temperature field and the electric field synchronously in various circumstances such as changing in ambient parameters or flowing current provides vital information in the design of reliable cables for electric aircraft. Also, the electric conductivity and electric field across the cable insulation are evaluated at different conductor currents and insulator temperature gradients.

II. MODEL

The thermal model of the study contains two parts, 1) conductive heat transfer from the core conductor of a 5 kV DC NL-EPR cable manufactured by Southwire, to the surface of the cable, and 2) conductive, convection, and radiation heat transfer from the surface of the cable to the ambient environment.

Table 1 presents the geometrical characteristics of the cable components [26]. The rated temperature of the cable for normal operation is 105°C, which counts as a thermal limit for the normal application of the cable. The specific parameters of containing materials of the model are presented in Table 2 [27] and [28].

TABLE 2. Specific parameters of material of the cable [27], [28].

Parameters	NL-EPR	PVC
Thermal Conductivity (W.(m.K)$^{-1}$)	0.3	0.19
Heat Capacity (J.(Kg.K)$^{-1}$)	1800	1050
Density (Kg.m^{-3})	860	1350
Surface Emissivity	-	0.91

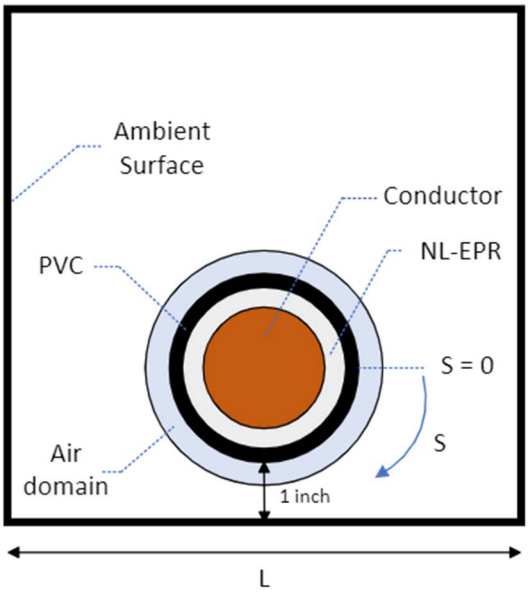

FIGURE 1. The FEM model of the study.

A coupled model of laminar flow, surface-to-surface heat radiation, and heat transfer is used to determine the maximum current flowing through the cable regarding its thermal limit at atmospheric and 18.8 kPa pressure. Also, to determine the electric field across the cable insulator a coupled model of heat transfer and electric currents has been conducted.

The FEM model of the study is shown in Fig. 1. To obtain the natural heat convection, a cylindrical air domain with a thickness of 0.35 inches is considered to enclose the cable. The thickness of the air domain is large enough that the effects of open boundary on the cable surface temperature can be ignored and small enough that the natural heat convection solution converged. The temperature of the outermost boundary of the air domain is considered equal to the ambient temperature.

Also, to model the heat transfer by radiation, a square-shaped domain with 1 mm thickness encloses the cable, representing the ambient surface. The ambient surface is an aluminum alloy with ambient temperature. The cable is placed at a 1-inch distance from one of the square-shaped domain sides. S and L are representing the length unit of the cable surface with the direction shown in Fig. 1 and the size of the square-shaped domain sides, respectively.

A. CONDUCTIVE HEAT TRANSFER

The heat transfer from the core conductor of the cable to its surface is only conductive. The heat transfer equation in the cable can be expressed as:

$$\rho C_p \frac{\partial T}{\partial t} + \nabla . (-k \nabla T) = Q + q_o \tag{1}$$

where ρ is the density (kg.m^{-3}), C_P is the specific heat capacity at the constant pressure (J.(kg.K)$^{-1}$), k is thermal conductivity (W.(K.m)$^{-1}$), T is the temperature (K), q_o is the net outward radiative heat flux (W. m^{-3}) and only applied to the outermost boundary of the cable where heat radiation occurs, and Q is the heat source (W.m^{-3}), which can be described as:

$$Q = Q_{con} + Q_{ins} \tag{2}$$

where Q_{con} and Q_{ins} are losses in the conductor and losses in the insulator. Q_{con} and Q_{ins} are respectively given by:

$$Q_{con} = I^2 R \tag{3}$$

$$Q_{ins} = \sigma E^2 \tag{4}$$

where I is the conductor current (A), R is the conductor resistance (Ω), σ is the insulator conductivity (S.m^{-1}), and E is the electric field norm in the insulator (V.m^{-1}).

The conductor losses (Q_{con}) is calculated by defining the conductor as a coil in the "Magnetic Fields" physics interface of COMSOL. The linear resistivity (ρ_e) of the coil is given by:

$$\rho_e = \rho_0 (1 + \alpha (T_C - T_{ref}) \tag{5}$$

where T_{ref} is the reference temperature (K), ρ_0 is the electric resistivity (Ω.m) at the reference temperature, α is the resistivity temperature coefficient (K^{-1}), and T_C is the conductor temperature (K).

Also, the insulation loses Q_{ins} is determined by the "Electric Current" physics interface of COMSOL in an approach that is described in Section II.D.

B. RADIATIVE HEAT TRANSFER

The surface-to-surface heat radiation is applied at the outermost boundary of the cable (outer radius of PVC jacket). Due to the cylindrical shape of the cable, considering P_1 is a point located on the surface of the cable, the net outward radiative heat flux (q_o) at P_1 is given by [29]:

$$q_o = \varepsilon_1 \left(E_{b1}(T) - G_{12} \right) \tag{6}$$

where ε_1 is the emissivity of the cable surface, G_{12} is the irradiation received at point P_1 from the ambient surface (W.m^{-2}), and $E_{b1}(T)$ is the power radiated across all wavelengths (W.m^{-2}) from P_1. $E_{b1}(T)$ can be expressed as [29]:

$$E_{b1}(T) = n^2 \sigma_S T_1^4 \tag{7}$$

where n is the refractive index of air ($n \approx 1$), σ_S is the Stefan's constant (W.m^{-2}K^{-4})), T_1 is the temperature of the point P_1 (K). Assuming the ambient surface is an isothermal surface, G_{12} is given by [29]:

$$G_{12} = F_{12} \left[\varepsilon_2 E_{b2}(T) + (1 - \varepsilon_2) G_{21} \right] \tag{8}$$

where ε_2 is the emissivity of the ambient surface, $E_{b2}(T)$ is the power radiated from the ambient surface (W.m^{-2}) and can

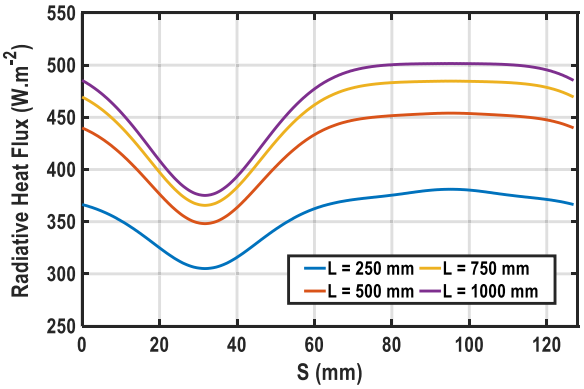

FIGURE 2. The radiative heat flux of the surface of the cable with a flowing current of 1200 A at the ambient temperature of 40°C with an ambient emissivity of 0.18.

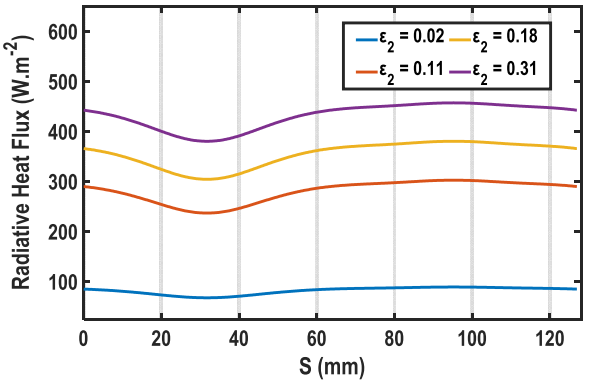

FIGURE 3. The radiative heat flux of the surface of the cable with a flowing current of 1200 A at the ambient temperature of 40°C when *L* is 250 mm.

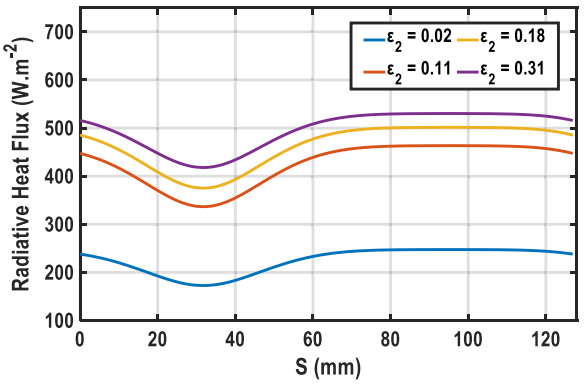

FIGURE 4. The radiative heat flux of the surface of the cable with a flowing current of 1200 A at the ambient temperature of 40°C when *L* is 1000 mm.

be obtained by replacing the ambient temperature in Eq. (7), G_{21} is the irradiation received at any point of the ambient surface from P_1 (W.m^{-2}), and F_{12} is the view factor and can be expressed as [30]:

$$F_{12} = \int_A \frac{cos\,\theta_1 cos\,\theta_2}{\pi R^2} dA \tag{9}$$

where R (m) is the line connecting any point on the ambient surface to P_1 without crossing the cable, θ_1 and θ_2 are polar angles formed by R with the surface normal of the cable and ambient surface, respectively, A is the surface area of the ambient surface (m^2), dA is the elemental area.

According to expressions (6), (8), and (9), q_o depends on the emissivity of the surfaces and geometry of the ambient surface (specifically L). By increasing L, the cable can be assumed a small convex object in a large cavity, leading to $F_{12} \approx 1$ [31]. Considering the cable surface temperature as 105°C and ambient temperature of 40°C, it can be predicted from (6) that the value of q_o increases by decreasing G_{12}, which in turn depends on the ambient surface emissivity and L.

Fig. 2 illustrates q_o of the cable surface with a temperature of 105°C, an ambient temperature of 40°C, and an ambient surface emissivity of 0.18, when L changes from 250 mm to 1000 mm. By increasing L, G_{12} decreases which in turn increases the cable surface radiative heat flux (q_o).

Another parameter that influences q_o is the emissivity of the aluminum alloy surface. The emissivity of aluminum surface is affected by many variables such as alloy composition, temperature, oxidation, and roughness. Its emissivity is 0.02 for unoxidized, 0.11 for oxidized, 0.18 for roughly polished, and 0.31 for heavily oxidized compositions [32].

Figs. 3 and 4 show q_o of the cable surface with a temperature of 105°C and an ambient temperature of 40°C when emissivity of the aluminum alloy surface varies for considering 250 mm or 1000 mm, respectively, as the extreme values for L. By increasing the emissivity of aluminum alloy surface, q_o significantly increases. Increasing of q_o at a constant temperature of the cable means that the maximum current flowing through the cable can be increased.

Therefore, it is desired to increase $\mathbf{q_o}$ by optimizing the values of the emissivity of the cable and ambient surface, and geometry of the ambient surface. Due to the moderate emissivity of the roughly polished aluminum alloy, this material is considered as the ambient surface in this study.

C. CONVECTIVE HEAT TRANSFER

The natural heat convection significantly affects the temperature of the cable. The heat equation in the air domain can be described as [33]:

$$\rho C_p \frac{\partial T}{\partial t} + \rho C_p u.\nabla T + \nabla.(-k\nabla T) = Q + q + \tau : \nabla u + \frac{-T}{\rho}\frac{\partial \rho}{\partial t}\left(\frac{\partial P}{\partial t} + u.\nabla P\right) \tag{10}$$

where ρ is the air density (kg.m^{-3}), C_p is the heat capacity at the constant pressure of the air (J.(kg.K)$^{-1}$), u is the air velocity vector (m.s^{-1}), k is the thermal conductivity of the air (W.(K.m)$^{-1}$), T is the temperature (K), τ is the viscous tensor (Pa), q is the heat flux (W.m^{-3}) and P is the pressure (Pa). The operator ":" stands for the double dot product,

which denotes a tensor contraction as defined by

$$a : b = \sum_{n} \sum_{m} a_{nm} b_{nm} \tag{11}$$

Also, τ can be expressed as [33]:

$$\tau = \mu \left(\nabla u + (\nabla u)^T \right) - \frac{2}{3} \mu \left(\nabla . u \right) I_I \tag{12}$$

where I_I is the identity matrix and μ represents the air's dynamic viscosity (kg.(m.s)$^{-1}$). The fluid (here air) velocity field can be determined from the momentum equation and the equation of continuity that are respectively expressed as [33]:

$$\rho \frac{\partial u}{\partial t} + \rho \left(u . \nabla \right) u = \nabla . \left(-P I_I + \tau \right) + \left(\rho - \rho_{ref} \right) g \tag{13}$$

$$\frac{\partial \rho}{\partial t} + \nabla . \left(\rho u \right) = 0 \tag{14}$$

where ρ_{ref} is the reference density (kg.m^{-3}), and g is the acceleration of gravity (m.s^{-2}).

The heat flux (q) at the outermost boundary of the cylindrical air domain for an outgoing flow across the boundary can be described as

$$q = 0 \tag{15}$$

Also, for an incoming flow across the boundary, the boundary condition is given by

$$q = -\rho u \Delta H \tag{16}$$

where ρ is the fluid density (kg.m^{-3}), ΔH is the enthalpy variation between the upstream conditions and inlet conditions, and u is the velocity vector (m.s^{-1}). ΔH can be expressed as

$$\Delta H = \int_{T_{up}}^{T} C_p dt + \int_{P_{up}}^{P} \frac{1}{\rho} \left(1 - \alpha_P T \right) dt \tag{17}$$

where T_{up} and P_{up} are respectively the upstream temperature (K) and upstream pressure (Pa), T and P are respectively the inlet temperature (K) and inlet pressure (Pa), ρ is the fluid density (kg.m^{-3}), and α_P is the coefficient of thermal expansion (K^{-1}). T_{up} equals to the ambient temperature. Considering air as an ideal gas, its density is given by

$$\rho = \frac{P}{RT} \tag{18}$$

where P is the pressure of the gas (Pa), T is the temperature of the gas (K), and R is the universal gas constant.

Expressions (10), (13), (14), and (18) show that the temperature field and the velocity field of the air, which are significantly depending on the air density, are coupled. At the altitude of 12.2 km, which is a typical altitude of cruising aircraft, and a temperature of 15°C, air pressure is 18.8 kPa and air density is 0.22 kg.m^{-3} compared to air density of 1.225 kg.m^{-3} at atmospheric pressure. Therefore, the temperature field and electric field distribution across the cable at the reduced pressure of 18.8 kPa will be different from its at atmospheric pressure.

The natural heat convection can experience laminar or turbulent flow conditions. To characterize the nature of the flow (Laminar or Turbulent), the Grashof number is used. It expresses the relationship between the time scales for viscous diffusion in a fluid and the buoyancy force [31].

For a long horizontal cylinder, the Grashof number can be described as [31]:

$$Gr_L = \frac{g \beta (T_s - T_{ext}) D^3}{v^2} \tag{19}$$

where β is the coefficient of thermal expansion (K^{-1}), g is the acceleration of gravity (m.s^{-1}), T_s and T_{ext} are temperatures of the hot surface and the free stream, respectively, v is the kinematic viscosity (m^2.s^{-1}), and D is the diameter of the long horizontal cylinder (m). The material data are evaluated at the average temperature of the surface and ambient. Although the maximum temperature in the cable occurs at the core conductor, considering the surface temperature of the cable as the rated temperature of the cable (105°C) and the free stream temperature as −35°C, and with the cable overall diameter mentioned in Table 1, the Grashof number will not exceed the critical number of 10^9, where the flow shifts from laminar to turbulent. Therefore, the laminar flow is chosen to model the fluid flow in the thermal model.

D. ELECTRIC CONDUCTIVITY AND ELECTRIC FIELD

The electric field in polymeric DC cables is a strong function of conductivity. In turn, conductivity depends on temperature field, electric field, and material of the insulation. Generally, The EPR conductivity can be expressed by empirical formulas such as [21], [34], and [35]:

$$\sigma \left(E, T \right) = \sigma_0 exp \left(\alpha T + \beta E \right) \tag{20}$$

$$\sigma \left(E, T \right) = \sigma_0 exp \left(\frac{-a}{T} + bE \right) \tag{21}$$

$$\sigma \left(E, T \right) = A exp \left(\frac{-\varphi q_e}{k_b T} \right) \frac{\sinh \left(B(T) \mathrm{E} \right)}{E^{\gamma}} \tag{22}$$

$$\sigma \left(E, T \right) = A exp \left(\frac{-\varphi q_e}{k_b T} \right) \frac{\sinh \left(B(T) \ln \left(E \right) \right)}{E^{\gamma}} \tag{23}$$

where α and a are temperature coefficients, β and b are the field coefficients, φ is the thermal activation energy, q_e is the electron charge, k_b is the Boltzmann's constant, σ_0, A and γ are polymeric material-related constants, and $B(T)$ is a temperature-dependent parameter given by

$$B \left(T \right) = cT + d \tag{24}$$

where c and d are polymeric material-based constants.

Expressions (20) and (21) result in errors when used in the calculation of electric field of DC cables. Expression (22) is more accurate than expressions (20) and (21) for a wide range of temperatures. However, in [35] it was shown that expression (23) yields more precise results for a wide range of electric fields and temperatures applied to an EPR insulation. Therefore, in this paper, expression (23) is chosen to model insulation conductivity. Table 3 presents parameters

TABLE 3. Conductivity parameters of equation (23) for EPR [35].

Parameters	φ (eV)	A (S.m^{-1})	c (K^{-1})	d	γ
Value	0.6	5.47015.10^{-9}	0.0065	-1.17	0.23

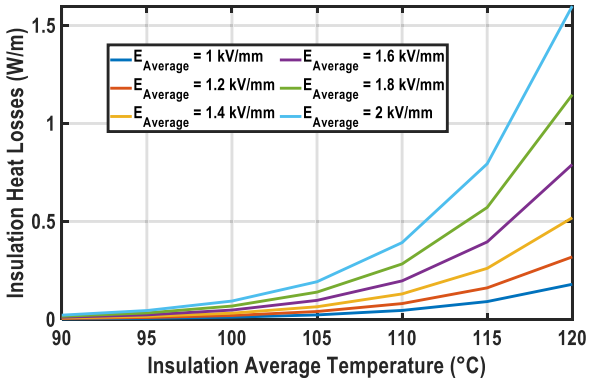

FIGURE 5. Insulation Heat losses for different insulation average electric fields at different insulation average temperatures.

φ, A, $B(T)$, and γ [35]. Using expressions (4) and (23), the insulation losses can be described as a function of the electric field norm and temperature.

Although the insulation losses (Q_{ins}) remains insignificant for the insulator temperatures below 105°C, as shown in Fig. 5, calculating it will enhance the thermal model accuracy.

The electric field distribution can be obtained by

$$E = -\nabla V \tag{25}$$

$$J = \sigma E \tag{26}$$

where E is the electric field (V.m^{-1}), V is the voltage (V), J is the current density (A.m^{-2}), and σ is the conductivity (S.m^{-1}).

As seen from Eqs. (1)-(26), the temperature field, velocity field, and electric field are coupled. The multi-physics model developed in the paper based on the aforementioned equations is used to obtain the maximum permissible current flowing through the cable at the pressure of 18.8 kPa. To obtain the steady case, the simulation time is 30 hours.

III. SIMULATION RESULTS

As discussed before, the temperature field, velocity field, and electric field are coupled. The size of the square-shaped domain surrounding the cable affects the cable temperature field by changing the total net outward radiative heat flux of the cable surface. Also, the air density, which is a function of the pressure and temperature of the air, influences the heat equation, momentum equation, and continuity equation. Therefore, the pressure of the air affects the convective heat transfer importantly.

Fig. 6 shows the maximum permissible flowing current of the cable at the pressure of 1 atmosphere and 18.8 kPa regarding the thermal limit of 105°C when the ambient temperature varies from −35°C to 65°C. As seen in Fig. 6, the maximum permissible current reduces in the entire range of

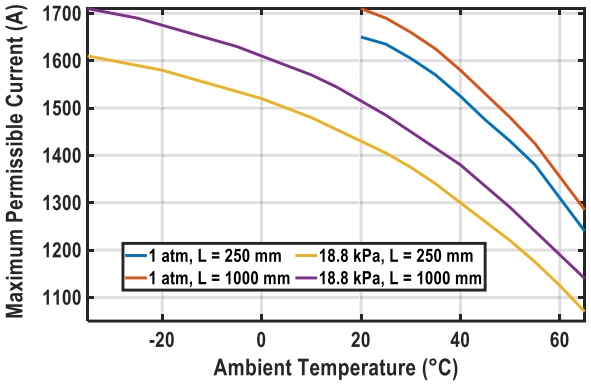

FIGURE 6. The maximum permissible current flowing through the cable.

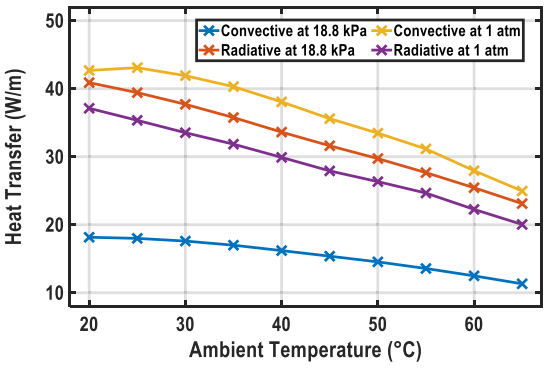

FIGURE 7. The heat transferred by convection when L is 250 mm.

ambient temperature due to the heat transfer limited by convection. The maximum reduction in maximum permissible current occurs at the ambient temperature of 55°C where the maximum permissible current at the pressure of 18.8 kPa compared to atmospheric pressure reduces by 14.8% when L is 250 mm and 13% when L is 1000 mm.

Figs. 7 and 8 illustrate the heat flux when the ambient temperature varies from 20°C to 65°C, at the atmospheric pressure and 18.8 kPa, when L equals 250 mm and 1000 mm, respectively. At an ambient temperature of 55°C, the amount of heat transfer by convection at 18.8 kPa is 56.5% lower than it at atmospheric pressure for both values of L. The maximum reduction in heat transfer by convection occurred at 25°C where its value at the 18.8 kPa pressure decreased by 58.3% compared to atmospheric pressure. Since the conductor temperature and conductive heat transfer in the cable remain constant for different pressures, the cable surface temperature and heat transfer by radiation change slightly, as shown in Figs. 7 and 8. Therefore, the reduction in heat transfer by convection is the main reason that the maximum permissible current is decreased at a reduced pressure of 18.8 kPa.

As it is expected, the maximum temperature in the cable occurs at the core conductor when the cable is operating under its thermal limit. Figs. 9 and 10 illustrate the temperature field across the cable at an ambient temperature of 40°C and

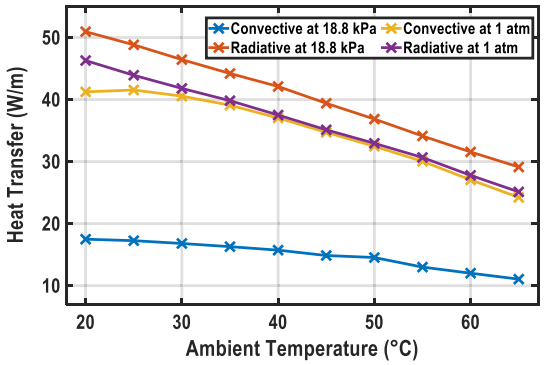

FIGURE 8. The heat transferred by convection when L is 1000 mm.

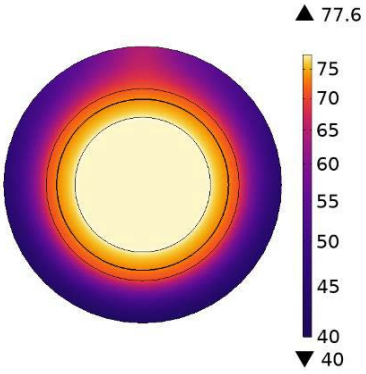

FIGURE 9. The temperature field (K) across the cable flowing current of 1000 A at an ambient temperature of 40°C and pressure of 18.8 kPa when L is 250 mm.

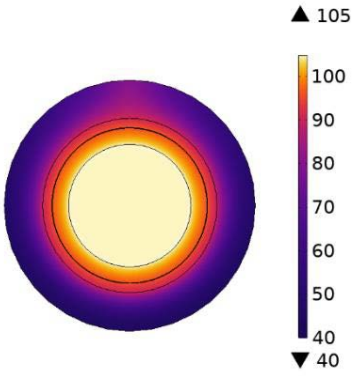

FIGURE 10. The temperature field (K) across the cable flowing current of 1300 A at an ambient temperature of 40°C and pressure of 18.8 kPa when L is 250 mm.

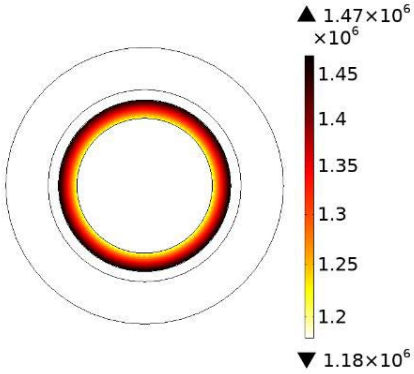

FIGURE 11. The electric field (V/m) across the cable flowing current of 1000 A at an ambient temperature of 40°C and pressure of 18.8 kPa when L is 250 mm.

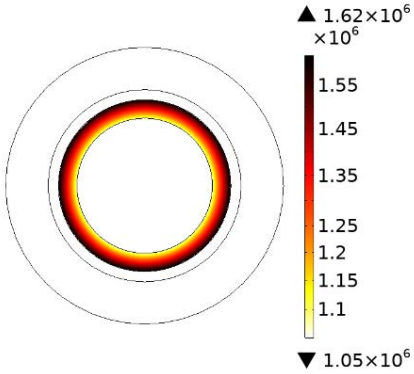

FIGURE 12. The electric field (V/m) across the cable flowing current of 1300 A at an ambient temperature of 40°C and pressure of 18.8 kPa when L is 250 mm.

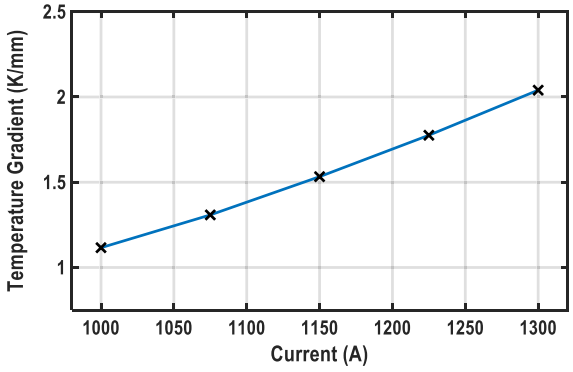

FIGURE 13. The temperature gradient across the insulation at the ambient temperature of 40°C and pressure of 18.8 kPa when L is 250 mm.

pressure of 18.8 kPa when the flowing current of the cable is 1000 A and 1300 A, respectively, for **L** equals 250 mm.

Temperature of most of the insulation layer and all the jacket remains below 100°C. Moreover, the temperature gradient across the insulation when the flowing current of the cable is 1300 A is larger than the flowing current of 1000 A. The temperature gradient across the insulation results in electric field inversion. The electric field inversion is intensified when the temperature gradient is larger, as shown in Figs. 11 and 12. Also, Figs. 13, 14, and 15 illustrate the temperature gradient, electric conductivity gradient, and electric field, respectively, across the insulation, when the flowing current varies from 1000 A to 1300 A at the ambient temperature of 40°C and pressure of 18.8 kPa when L is 250 mm. Increasing the cable current results in increasing the temperature gradient and electric conductivity gradient. Consequently, the electric field inversion is intensified when

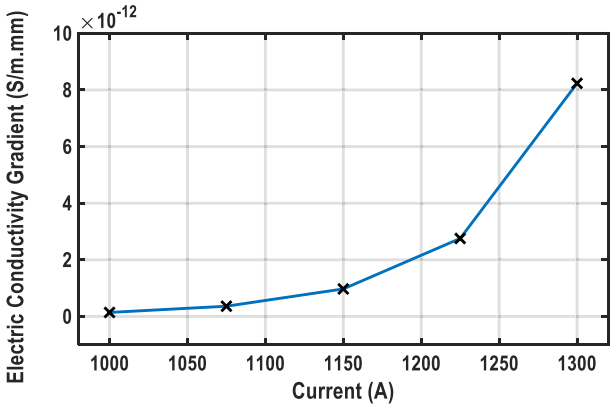

FIGURE 14. The electric conductivity gradient across the insulation at the ambient temperature of 40°C and pressure of 18.8 kPa when *L* is 250 mm.

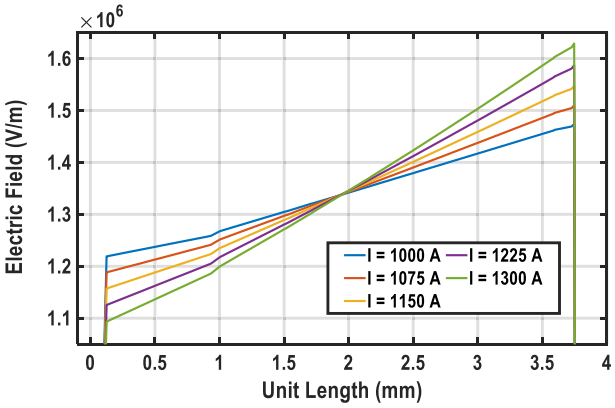

FIGURE 15. The electric field distribution across the insulation at the ambient temperature of 40°C and pressure of 18.8 kPa when *L* is 250 mm.

the flowing current increases. However, the electric field across the cable is less than dielectric breakdown strength of the insulation, so the cable is safe in terms of electrical insulation performance under normal operation.

IV. CONCLUSION

For the first time, a coupled electrical, thermal, and fluid flow model was built in this work to obtain the temperature field and electric field of a 5 kV DC power aircraft cable. The model was used to obtain the maximum permissible current flowing the cable at the cruising altitude (at a low pressure of 18.8 kPa) of envisaged wide body all electric aircraft. The results show that at the ambient temperature of 55°C and low pressure of 18.8 kPa the maximum permissible current of the cable considered in this study should be decreased by 14.8% and 13% for the ambient surface side size of 250 mm and 1000 mm, respectively, compared to the maximum permissible current of the cable at atmospheric pressure. Also, it was shown that at a low pressure of 18.8 kPa the heat transfer by convection decreases by 57.5% and 58.3% for the ambient temperature of 55°C and 25°C, respectively, compared to its value at atmospheric pressure. In addition, regarding the temperature gradient and electric conductivity gradient across the insulation, the electric field was studied. The electric field inversion is intensified when the temperature gradient and electric conductivity gradient across the cable insulation are larger. The results of this study show that due to the limited heat transfer by convection for aircraft applications, the current commercial power cables cannot operate at their maximum ampacity. Therefore, for aircraft applications, the existing commercial power cables should work at lower ampacities than their nominal ampacity, or new designs should be developed. The coupled FEM model of this paper lays grounds for further research in designing high-temperature and low-density power cables for aircraft applications.

REFERENCES

[1] A. Barzkar and M. Ghassemi, "Electric power systems in more and all electric aircraft: A review," *IEEE Access*, vol. 8, pp. 169314–169332, 2020.

[2] H. Schefer, L. Fauth, T. H. Kopp, R. Mallwitz, J. Friebe, and M. Kurrat, "Discussion on electric power supply systems for all electric aircraft," *IEEE Access*, vol. 8, pp. 84188–84216, 2020.

[3] A. Barzkar and M. Ghassemi "Components of electrical power systems in more and all-electric aircraft: A review," *IEEE Trans. Transport. Electrific.*, vol. 8, no. 4, pp. 4037–4053, Dec. 2022.

[4] M. Ghassemi, A. Barzkar, and M. Saghafi, "All-electric NASA N3-X aircraft electric power systems," *IEEE Trans. Transport. Electrific.*, vol. 8, no. 4, pp. 4091–4104, Dec. 2022.

[5] M. Ghassemi and A. Barzkar, "DC load flow models for the electric power system of wide body all electric aircraft," in *Proc. IEEE Aerosp. Conf. (AERO)*, Big Sky, MT, USA, Mar. 2022, pp. 1–8.

[6] M. Ghassemi and M. Saghafi, "Optimal electric power system architectures for wide body all electric aircraft," in *Proc. IEEE Aerosp. Conf. (AERO)*, Big Sky, MT, USA, Mar. 2022, pp. 1–9.

[7] M. Ghassemi and A. Barzkar, "Power flow solvers for medium voltage direct current (MVDC) microgrids," in *Proc. 6th IEEE Workshop Electron. Grid (eGRID)*, Nov. 2021, pp. 1–6.

[8] H. El Bayda, F. Valensi, M. Masquere, and A. Gleizes, "Energy losses from an arc tracking in aeronautic cables in DC circuits," *IEEE Trans. Dielectr. Electr. Insul.*, vol. 20, no. 1, pp. 19–27, Feb. 2013.

[9] A. Gleizes, "The problem of electric arcs in aeronautics," in *Proc. 18th Symp. Phys. Switching Arc*, Brno, Czech Republic, 2013, p. 27.

[10] F. Dricot and H. J. Reher, "Survey of arc tracking on aerospace cables and wires," *IEEE Trans. Dielectr. Electr. Insul.*, vol. 1, no. 5, pp. 896–903, Oct. 1994.

[11] G. C. Montanari, P. Seri, S. F. Bononi, and M. Albertini, "Partial discharge behavior and accelerated aging upon repetitive DC cable energization and voltage supply polarity inversion," *IEEE Trans. Power Del.*, vol. 36, no. 2, pp. 578–586, Apr. 2021.

[12] H. Naderiallaf, P. Seri, and G. C. Montanari, "Investigating conditions for an unexpected additional source of partial discharges in DC cables: Load power variations," *IEEE Trans. Power Del.*, vol. 36, no. 5, pp. 3082–3090, Oct. 2021.

[13] C. Emersic, R. Lowndes, I. Cotton, S. Rowland, and R. Freer, "The effects of pressure and temperature on partial discharge degradation of silicone conformai coatings," *IEEE Trans. Dielectr. Electr. Insul.*, vol. 24, no. 5, pp. 2986–2994, Oct. 2017.

[14] G. J. Anders, *Rating of Electric Power Cables in Unfavourable Thermal Environment*. Hoboken, NJ, USA: Wiley, 2005.

[15] *Wiring Aerospace Vehicle*, Standard AS50881, 2006.

[16] M. Fu, L. A. Dissado, G. Chen, and J. C. Fothergill, "Space charge formation and its modified electric field under applied voltage reversal and temperature gradient in XLPE cable," *IEEE Trans. Dielectr. Electr. Insul.*, vol. 15, no. 3, pp. 851–860, Jun. 2008.

[17] D. Fabiani, G. C. Montanari, C. Laurent, G. Teyssedre, P. H. F. Morshuis, R. Bodega, and L. A. Dissado, "HVDC cable design and space charge accumulation. Part 3: Effect of temperature gradient [feature article]," *IEEE Elect. Insul. Mag.*, vol. 24, no. 2, pp. 5–14, Mar./Apr. 2008.

[18] M. Tefferi, M. A. Baferani, H. Uehara, and Y. Cao, "The correlation and balance of material properties for DC cable insulation at design field," *IEEE Access*, vol. 8, pp. 187840–187847, 2020.
[19] D. Fabiani, G. C. Montanari, C. Laurent, G. Teyssedre, P. H. F. Morshuis, R. Bodega, L. A. Dissado, A. Campus, and U. H. Nilsson, "Polymeric HVDC cable design and space charge accumulation. Part 1: Insulation/semicon interface," *IEEE Elect. Insul. Mag.*, vol. 23, no. 6, pp. 11–19, Nov. 2007.
[20] J. Yu, X. Chen, F. Meng, A. Paramane, and S. Hou, "Numerical analysis of thermo-electric field for AC XLPE cables with different service times in DC operation based on conduction current measurement," *IEEE Trans. Dielectr. Electr. Insul.*, vol. 27, no. 3, pp. 900–908, Jun. 2020.
[21] T. T. N. Vu, G. Teyssedre, B. Vissouvanadin, S. L. Roy, and C. Laurent, "Correlating conductivity and space charge measurements in multi-dielectrics under various electrical and thermal stresses," *IEEE Trans. Dielectr. Electr. Insul.*, vol. 22, no. 1, pp. 117–127, Feb. 2015.
[22] J. Gu, X. Li, and Y. Yin, "Calculation of electric field and temperature field distribution in MVDC polymeric power cable," in *Proc. IEEE 9th Int. Conf. Properties Appl. Dielectric Mater.*, Jul. 2009, pp. 105–108.
[23] G. Rizzo, P. Romano, A. Imburgia, and G. Ala, "Partial discharges in HVDC cables—The effect of the temperature gradient during load transients," *IEEE Trans. Dielectr. Electr. Insul.*, vol. 28, no. 5, pp. 1767–1774, Oct. 2021.
[24] A. Azimuddin and S. S. Refaat, "A comprehensive model for electrical degradation of power cable insulation," in *Proc. IEEE Conf. Electr. Insul. Dielectric Phenomena (CEIDP)*, Dec. 2021, pp. 133–138.
[25] U. Farooq, F. Yang, J. A. Shaikh, M. S. Bhutta, F. Aslam, W. Tao, L. Jinxian, and I. U. Haq, "Temperature field simulation and ampacity optimization of 500 kV HVDC submarine transmission cable," in *Proc. Int. Conf. Adv. Electr. Equip. Reliable Operation (AEERO)*, Oct. 2021, pp. 1–6.
[26] Southwire Company LLC. *SPEC 46102*. Accessed: Oct. 6, 2022. [Online]. Available: https://assets.southwire.com/ImConvServlet/imconv/2ad2616bcd904a52757faccf04007a9948ae9bef/origin?assetDescr=1-C%20CU%205kV%20115%20NLEPR%20133%20percent%20SIMpull%20%20PVC%20MV-105.spec
[27] X. Qi and S. Boggs, "Thermal and mechanical properties of EPR and XLPE cable compounds," *IEEE Elect. Insul. Mag.*, vol. 22, no. 3, pp. 19–24, May 2006.
[28] A. S. Chepurnenko, S. B. Yazyev, and A. I. Evtushenko, "Non-stationary temperature field modeling in electric cable with PVC insulatio," in *Proc. Int. Conf. Ind. Eng., Appl. Manuf. (ICIEAM)*, May 2017, pp. 1–4.
[29] R. Siegel and J. Howell, *Thermal Radiation Heat Transfer*, 4th ed. New York, NY, USA: Taylor & Francis, 2002.
[30] M. F. Modest, *Radiative Heat Transfer*, 2nd ed. San Diego, CA, USA: Academic, 2003.
[31] F. P. Incropera and D. P. DeWitt, *Fundamentals of Heat and Mass Transfer*, 5th ed. New York, NY, USA: Wiley, 2002.
[32] M. Ghane and E. Ghorbani, "Investigation into the UV-protection of woven fabrics composed of metallic weft yarns," *Autex Res. J.*, vol. 16, no. 3, pp. 154–159, Sep. 2016.
[33] R. L. Panton, *Incompressible Flow*, 2nd ed. Hoboken, NJ, USA: Wiley, 1996.
[34] C. C. Reddy and T. S. Ramu, "On the DC conductivity of HV DC cable insulation–cautions in using the empirical models," in *Proc. Conf. Rec. IEEE Int. Symp. Electr. Insul.*, Jun. 2008, pp. 39–42.
[35] L. V. Taranu, P. Notingher, and C. Stancu, "Dependence of electrical conductivity of ethylene-propylene rubber on electric field and temperature," *Rev. Roum. Sci. Techn.*, vol. 63, pp. 243–248, Jul. 2018.

ARIAN AZIZI (Member, IEEE) received the B.Sc. degree from Shahid Beheshti University, Tehran, Iran, in 2016, and the M.Sc. degree from the University of Tehran, Tehran, in 2020, both in electrical engineering. He is currently pursuing the Ph.D. degree with the ECE Department, The University of Texas at Dallas, TX, USA.

His research interests include power systems, power electronics, high voltage engineering, and electrical insulation.

MONA GHASSEMI (Senior Member, IEEE) received the B.Sc. degree from Shahed University, Tehran, Iran, in 2004, and the M.Sc. and Ph.D. degrees (Hons.) in electrical engineering from the University of Tehran, Tehran, in 2007 and 2012, respectively.

From 2013 to 2015, she was a Postdoctoral Fellow at the NSERC/Hydro-Quebec/UQAC Industrial Chair on Atmospheric Icing of Power Network Equipment (CIGELE), University of Québec at Chicoutimi (UQAC), Chicoutimi, QC, Canada. She was also a Postdoctoral Fellow at the University of Connecticut, Storrs, CT, USA, from 2015 to 2017. In 2017, she joined the Bradley Department of Electrical and Computer Engineering, Virginia Tech, Blacksburg, VA, USA, as an Assistant Professor. In 2021, she was named both the Steven O. Lane Junior Faculty Fellow and the College of Engineering Faculty Fellow at Virginia Tech. In 2022, she joined as an Associate Professor with tenure (early tenure) at the Department of Electrical and Computer Engineering, The University of Texas at Dallas. She has been the Chairholder of the Texas Instruments Early Career Award, since 2022. She has been a Registered Professional Engineer, since 2015. She has authored more than 110 peer-reviewed journals and conference papers and one book chapter. Her research interests include transportation electrification, clean energy, electrical insulation materials and systems, high voltage/field engineering and technology, power systems, plasma science, and power electronics.

Dr. Ghassemi is an At-Large Member of the Administrative Committee of the IEEE Dielectrics and Electrical Insulation Society (DEIS), DEIS-Representative in IEEE USA Public Policy Committee on Transportation and Aerospace Policy (CTAP), a Corresponding Member of the IEEE Conference Publication Committee of the IEEE Power and Energy Society (PES), an Active Member of several CIGRE working groups and IEEE Task Forces, and a member of the Education Committee of the IEEE DEIS and PES. She received three most prestigious, most competitive career awards, which are the 2021 Department of Energy (DOE) Early Career Research Program Award, the 2020 National Science Foundation (NSF) CAREER Award, and the 2020 Air Force Office of Scientific Research (AFOSR) Young Investigator Research Program (YIP) Award. She received the 2020 Contribution Award from the *IET High Voltage Journal* and also received four Best Paper Awards. She is an Associate Editor of IEEE Transactions on Dielectrics and Electrical Insulations, IEEE Transactions on Industry Applications, *High Voltage* (IET), *International Journal of Electrical Engineering Education*, and *Power Electronic Devices and Components* (Elsevier), and a Guest Editor of *Energies*.

JANE M. LEHR (Fellow, IEEE) received the B.E. degree in engineering physics from the Stevens Institute of Technology, Hoboken, NJ, USA, in 1985, and the Ph.D. degree in electrical engineering from New York University, New York, NY, USA, in 1996.

She was a Research Scientist at the Air Force Research Laboratory's Directed Energy Directorate, Kirtland AFB, NM, USA, Sandia National Laboratories, Albuquerque, NM, USA, and industry. She joined The University of New Mexico, Albuquerque, in 2013, where she currently runs the Advanced Pulsed Energy, Ionization and Discharge Center (APERIODIC), Department of Electrical and Computer Engineering.

Dr. Lehr was the President of the IEEE Nuclear and Plasma Sciences Society, from 2007 to 2008, and remains active on ExCom and AdCom, where she is currently supporting IEEE Fellow Nomination and has recently been named as a Distinguished Lecturer.